Snap-Through Morphogenesis in Thin-Shell Space Structures: From Concept to Scalability

Siamand Lalisani*, Fabien Royer†
Sibley School of Mechanical and Aerospace Engineering, Cornell University, 124 Hoy Rd, Ithaca, 14850 NY, USA

We present a novel programmable structure which can be shaped directly on-orbit through elastic buckling in a new hybrid in-space assembly and manufacturing (ISAM) process. This process takes inspiration from recently proposed in-space deformation processing and enables the shaping of ultra-thin composite deployable booms to create large space structures. The design concept uses bistable unit cells as building blocks for a cellular deployable meta-structure that can transition between multiple stable configurations through the trigger of snap-through instabilities in a sequence of cells. This study investigates the conditions for which the individual cells and the full meta-structure become multistable, highlighting the influence of stiffness, geometry, and target cell location on achievable deformed configurations. Another aspect of the paper is the exploration of the scalability and programmability of this cellular architecture, which enables a single structure to adaptively meet a wide range of mission requirements, ranging from large deployable reflectors to reconfigurable antennas and structural booms for space infrastructures. By applying various actuation strategies, the structure's shape can be precisely reconfigured to achieve a wide range of geometries, such as curved circular beams of varying radii or S-shaped profiles. This work offers a proof of concept for designing and assembling complex, large ultra-lightweight space structures with minimal power consumption.

I. Introduction

In an era of global warming, there is a pressing need for the next generation of spacecraft to focus on an extremely important mission: supporting human life on Earth. This goal can be achieved through developing large radiometry satellites that can enhance climate modeling and improve natural disaster forecasting [1, 2], or designing giant space solar power satellites that can collect sunlight and transfer energy on demand to any location on Earth [3]. These missions will help mitigate ecological disasters and foster renewable energies while offering an alternative to fossil fuels. The main facilitator of these future space missions is ultra-lightweight, large space structures that enable the creation of large microwave reflectors, antennas, and sunlight collectors [4]. The challenges in designing large space structures

Presented as Paper 2025-0690 at the AIAA SciTech, Orlando, FL,January 6–10, 2025.
*PhD Student, Sibley School of Mechanical and Aerospace Engineering, Cornell University. AIAA Student Member.
†Assistant Professor, Sibley School of Mechanical and Aerospace Engineering, Cornell University, fabienr@cornell.edu. AIAA Member (Corresponding Author).

include maintaining a high surface accuracy [5] and the limited volume capacity of existing launch system fairings. A recent study highlighted that even with the largest rockets currently being envisioned today, tightly-packaged mesh reflectors would exceed packaging constraints for diameters above a hundred meters [6]. One recommended solution to pushing the limits of aperture size is in-space manufacturing and assembly (ISAM). ISAM has been employed as a solution for manufacturing parts in space [7] and for assembling antennas and lenses in NASA's On-orbit Servicing, Assembly, and Manufacturing (OSAM-1 and OSAM-2) projects [8].

ISAM processes could overcome size constraints imposed by rocket fairings by directly manufacturing antennas in space from tightly packaged feedstock. However, today's ISAM concepts suffer from severe limitations that prevent their use at large scales. In-space manufacturing concepts feature a high power consumption, which dramatically reduces their build rates, and large masses, which make structures hard to control once manufactured [9]. On the other hand, in-space assembly often requires multiple robots interacting with flexible structures [10], which presents risks and operational challenges that remain unresolved.

An innovative concept proposed to overcome the limitations of designing and creating large space structures is in-space deformation processing [11]. In this method, the structure is processed into a desired shape through plastic deformations [12]. While this process requires less energy compared to in-space manufacturing, and can accelerate the on-orbit creation of structures, it also features its own set of limitations. Deformation processing relies on high density ductile materials [13], which reduces the structure's mass efficiency and first natural frequency. Additionally, controlling such a heavy structure during manufacturing and mission operations presents considerable challenges caused by large changes in inertial properties during the building process [14] and low natural frequencies [15].

To address these issues, our solution employs a hybrid approach combining in-space manufacturing and in-space assembly. It integrates recent advances in deformation processing with proven deployable structure technology [16–18] to circumvent conventional ISAM power and mass limitations. This new process utilizes lightweight composite deployable booms, whose shape can be programmed during deployment through elastic buckling. This new deformation processing paradigm effectively replaces plastic deformations by structural instabilities as shaping mechanism, which enables the very low-power forming of ultra-lightweight brittle fiber composites. In particular, we employ a deployable feedstock made of a periodic bistable cell arrangement. Snap-through buckling can be induced in selected cells during deployment, which in turns generate global curvature in the deployed structure.

The paper is organized as follows. Section II introduces the new snap-through shaping concept. The framework for finite element modeling and the problem geometry are then presented in Section III. The bistable behavior of a single unit cell, as a building block of a cellular structure, is studied in Section IV.A.1, and the snap-through transition of the full feedstock meta-structure is described in Section IV.A.2. Sections IV.B.1, IV.B.2 and IV.B.3 discuss different pinching strategies and scalability of the the concept. Also the programmability of structure is studied in Section IV.C. Finally, Section V concludes the paper and offers insights into future research directions.

II. Concept

Our new ISAM concept takes advantage of the low-power characteristic of deformation processing while addressing its mass limitations. In this new approach, we change the mechanism by which the feedstock is shaped, from plastic deformations to elastic buckling. To do so, we engineered a deployable feedstock meta-structure composed of a cellular array of unit cells. Each unit cell is formed by combining an upper and a lower arch, which feature a bistable behavior as previously studied in literature [19]. These cells can be selectively pinched by an actuator during on-orbit deployment to introduce local bends in the initially straight booms. In addition, multiple booms can be woven together by two deployment mechanisms located on the spacecraft, before being pinched to form large doubly-curved structures such as paraboloids. We envision programmability to be implemented through an algorithm that takes as input the reflector shape and returns a set of cells to collapse during deployment. The development of this algorithm is currently in progress and will be presented in a future study. The overall concept is illustrated in Figure 1.

Using programmable multistable structures has been investigated for instance for mechanical wave propagation [20], energy absorption [21] and harvesting [22], and in reconfigurable and shape morphing structures [23–27]. Wu and Pasini [28, 29] developed a multistable meta-material with a tunable topological state by employing an in situ snap-through buckling actuation mechanism, offering potential applications in vibration isolators with adjustable resonance frequencies. Mofatteh, Akbarzadeh, et al. [30] investigated a shape-reconfigurable meta-structure to control the release of elastic energy, aiming to uncover latent functionalities for designing architected materials and mechanical sensor-memory devices. Aveline, Santer, et al. [31] attempted to solve the inverse design of a unit cell to achieve a prescribed stress–strain response using topology optimization, and discovered a new lattice structure composed of bistable unit cells. Rahman et al. [32] have experimentally shown that arrays of bistable units, driven by elastic snap-through buckling, can be concatenated to achieve stable target shapes, providing a scalable approach for designing shape-retaining morphing structures.

Earlier concepts, for example the work of Santer and Pellegrino [33], investigated the use of bistable elements for shape-morphing structures such as compliant plates that deform elastically into different shapes and are able to maintain those shapes due to the presence of bistable components. Our work builds on a similar idea but adapts it to coilable structures. Specifically, the idea behind this project is using elastic ultra-thin shell arches that undergo snap-through buckling (collapse) when loaded to induce geometric frustration in a cellular network, causing it to bend. The cell geometry used in the structure can be chosen such that the collapsed state is a stable equilibrium configuration. This simple bistable component is then tessellated into cellular structures to create larger assemblies and meta-structure. By utilizing bistable cells as building blocks, these meta-structures could achieve the overarching goals of structural versatility and efficient in-space assembly. In this paper, a new architecture for a meta-structure is introduced that can smoothly reshape from a straight, deployable form into a defined shape in its second stable configuration. As described in Figure 1, a deployable cellular boom is coiled within a deployment and shaping mechanism. During deployment,

cells are selectively pinched to induce local buckling, enabling the structure to conform to a target second stable shape. Perpendicular deployment mechanisms weave multiple booms into a lattice, forming a large space structure, such as a microwave reflector. [34].

In large-scale applications, the stiffness-to-mass ratio is a key consideration. While this approach is expected to maintain a competitive stiffness-to-mass ratio at larger scales, its primary advantages are stowage efficiency, reconfigurability, and low built time. Existing deployable antennas, such as pantograph-based structures, face significant packaging limitations for apertures larger than 90 m [6] . The design presented in this paper addresses this limitation by enabling higher packaging efficiencies, similar to those found in coilable booms used in solar sails [35]. Trusses obtained through in-space assembly would be stiffer than the structures proposed in this article and enable the tensioning of larger reflectors. However, their assembly and control can be limited by inertia [14], which would yield larger build rates. The anticipated limited stiffness of the present concept may call for architectures that do not rely on membrane tensioning but rather distribute functionality on bending-stiff structures, as in [36]. Finally, while this concept does not offer as much design freedom as in-space manufacturing processes, its reliance on deformation processing would enable order of magnitude lower build times compared to traditional melt-based processes [9], and provide additional functionality through shape adaptability, such as beam steering. A quantitative comparison of this concept's performance with existing solutions is an important next step in this effort.

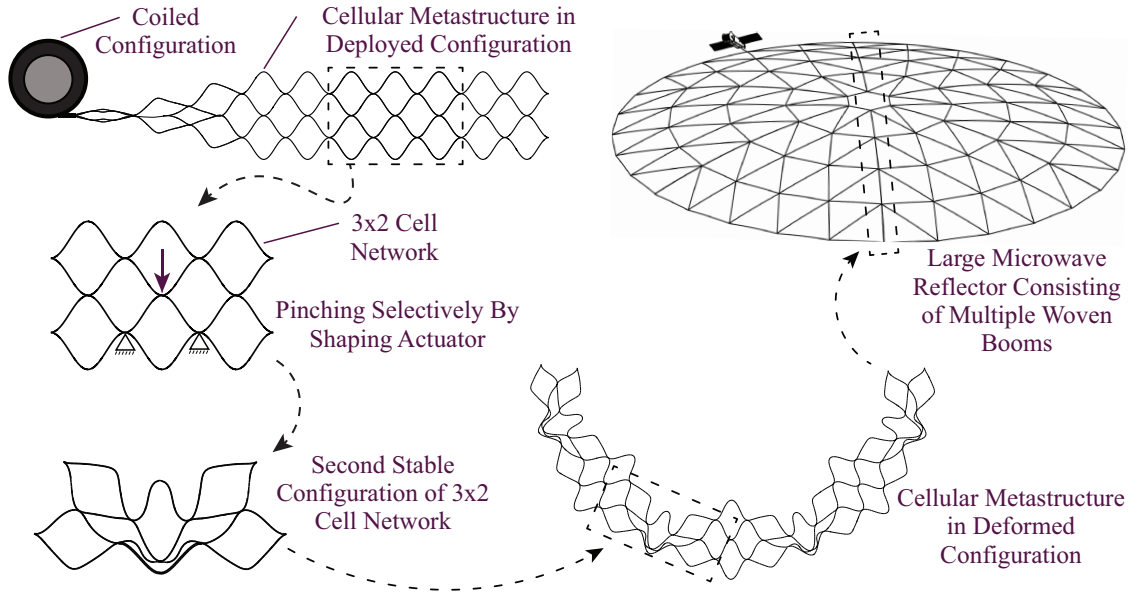


Fig. 1 Conceptual illustration of a deployable shape-programmable structure forming a large microwave reflector from a coiled configuration.

III. Methods

A. Finite Element Modeling

Finite element simulations are used to analyze the bistable behavior of this novel feedstock meta-structure. This study utilizes the commercial finite element software Abaqus 2023 and its Python scripting capabilities. Abaqus/Standard (implicit) is employed for the analysis. Boundary conditions are applied via reference points rigidly coupled to all nodes located on the edges of the target cells. The structure is meshed with rectangular reduced integration shell elements (S4R), with an average mesh edge size of 1 mm. The structure consists of fiber reinforced laminates made from 40 μm thick unidirectional carbon fiber reinforced plastic (CFRP, MR60H/PMT-F7) and 55 μm thick unidirectional glass fiber reinforced plastic (GFRP, S2/ Patz PMT-F7). We focus on a $[0]_n$unidirectional laminate in this study to isolate and directly study how the laminate's bending stiffness affect bistability, without the added complexity of varying the stacking sequences. While in practice, incorporating 90-degree fibers is necessary to prevent fiber splitting, one practical approach to achieving our simulated configuration in practice is to add a thin ply of Polyimide at the top and bottom of the laminate. This addition prevents fiber splitting in the transverse direction while having minimal impact on the laminate's overall bending stiffness. The material properties used in the finite element model are summarized in Table 1. It is important to highlight that for the cell geometry parametrized by Equation (1), contact between arches has a negligible effect on the snap-through response of the structure regardless of its aspect ratio and thickness (less than 1% relative error in reaction force between the two responses for the entire range of displacement). Therefore, for all simulations presented in this paper, no contact interactions were defined in Abaqus. However, this assumption will have to be revisited for different cell geometries. For instance, re-entrant geometries that use contact to increase the stability of the second stable state are currently being investigated, and require full contact definition to be accurately analyzed.

Table 1 Material properties used in finite element modeling.

	E_1 (GPa)	E_2 (GPa)	G_{12} (GPa)	ν_{12}	$t(\mu$m)
GFRP	55.0	5.5	6.4	0.26	55.2
CFRP	174.4	8.39	6.4	0.259	44.0

B. Geometry and Boundary Conditions

In this section, the structure's geometrical parameters, loading, and boundary conditions are described. First, it should be mentioned that the final goal of this study is to examine the bistable behavior of a cellular feedstock meta-structure composed of unit cells. Each cell consists of an upper and a lower arch, and the shape of the arches is given by the following equation [19]:

$$w_0(x) = \frac{h}{2}(1 - cos(\frac{2\pi x}{L})) \tag{1}$$

where x and w_0 are the horizontal and vertical coordinates respectively, h is the height, and L is the length of the arch. The depth of the arches is kept constant and equal to 50 mm in this study.

It has been shown in literature that a single arch will exhibit bistability when the projected length between its supports is fixed [37, 38]. This condition can be achieved using pinned-pinned boundary conditions on both sides. The action of these pin supports is often referred to as "confining stiffness." The idea behind this project is to harness the bistability of these arches without relying on an external system to enforce the boundary conditions. The proposed solution is to create a cell in which the top arch acts as the elastic arch undergoing snap-through, while the bottom arch provides the confining stiffness required for bistability, as explored in recent meta-material concepts [28, 29]. This design effectively mimics the effect of pinned boundary conditions for the upper cell.

Two types of analyses are conducted in our study: a single cell analysis and a meta-structure analysis. The single-cell analysis focuses on one of the identical cells that make up the meta-structure and aims to identify the design parameters that drive the cell's bistability. In the meta-structure study, we aim to address the following questions: Is it possible to design a more complex multistable structure using bistable unit cells? If so, how can we control the second stable configuration to achieve a desired shape?

The boundary conditions for the study of unit cells are defined as pin-roller supports, representing the support conditions of a unit cell within a meta-structure if the stiffness of the neighboring cells were to be ignored. For the meta-structure, the local boundary conditions for the target cell are roller-roller supports, while the global boundary conditions for the whole cell network are defined as pinned supports. A representation of the boundary conditions and other geometrical parameters are shown in Figure 2. By pushing the top arch of the target cell, with boundary conditions applied at the edges of the cellular structure, a global bending deformation is induced, which competes with the desired intended local cell deformation. To prevent this undesired deformation, the simulations are conducted in two steps. First, local roller boundary conditions are imposed around the target cell, and a displacement is applied to the top arch using the Abaqus Newton-Raphson solver (Static general), until the second stable state is reached. Next, a static general release step is defined, during which the local boundary conditions are replaced with global pinned support, allowing the structure to reconfigure and reach its global second stable state. This simulation process has practical implications for the design of a shaping actuator, which must be capable of providing the required local boundary conditions during the shaping process. The shaping actuator, currently in the prototyping phase in the laboratory, consists in an end-effector mounted on a 3-axes gantry similar to those found in compact FDM 3D printer. This gantry is attached to the end of the deployment mechanism which unfurl the structure in its straight configuration. The end-effector features two fixed cylindrical supports that approximate the target cell roller boundary conditions, and a small gripper provides the prescribed cell displacement. Note that the roller boundary conditions used in the paper model the type of supports that is most detrimental to bistability. In practice, friction between the cylindrical supports and the structure can provide additional confining stiffness which lowers the minimum load encountered during snap-through.

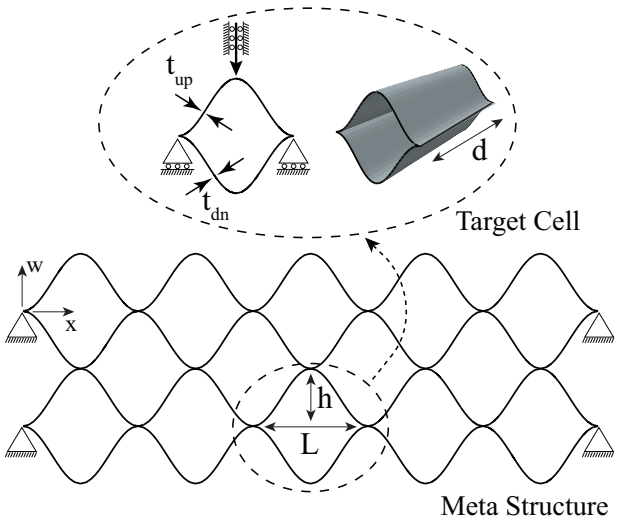


Fig. 2 Schematic of the meta-structure created by bistable unit cells.

IV. Results and Discussion

A. Multistability

1. Bistability of Unit Cell

We focus next on the study of the bistability of a single unit cell as a building block for the meta-structure. The top and bottom arches of the cell perform a different function, as described earlier. When the top cell is displaced downward, it undergoes snap-through. Whether the snap-through instability exhibit a second stable state depends on the confining stiffness produced by the bottom arch, i.e. its ability to limit the top arch's axial displacement (leading to flattening). We refer to the bistability threshold as the situation in which the cell transitions from being monostable to bistable without the need for external constraints. This single unit cell analysis is designed to isolate the effect of cell geometry by neglecting the compliance of the network and the influence of adjacent cells. In the subsequent section, we examine the combined effects of neighboring cells and boundary conditions on the bistability of the metastructure. This separation allows us to determine whether the loss of bistability observed at the network level originates from the geometry of the unit cell itself or from interactions with adjacent cells. The comparison between the two analyses can for instance inform whether some additional design features should be considered at the interfaces between cells, for example cutouts, or if the cell geometry should be changed.

In this section, the effect of the thickness ratio between the lower and upper arch on the bistability threshold is examined. In this analysis, the laminate of the upper arch is fixed to be a single $[0]_1$ composite ply, while the number of plies of the bottom arch layup is varied from $[0]_1$ to $[0]_5$. In addition, both CFRP, GFRP and a combination of these two materials are considered. The force versus displacement curve is analyzed when the cell is subjected to an imposed top arch displacement. The results for a GFRP cell with $L = 40$ mm, $h = 20$ mm, $h/L = 0.5$, $L/t_{up} = 720$,

are shown in Figure 3a where in the figure, D_{up} corresponds to the displacement applied at the apex of the upper arch, and F_{up} denotes the resulting reaction force. These curves clearly indicate that the cell only features bistability above of thickness ratio of 3, above which the bottom cell provides enough confining stiffness to create a second equilibrium state. The same analysis for CFRP and hybrid cells shows that the required thickness ratios are 3 and 2, respectively. This indicates that the bistability threshold is directly influenced by the stiffness of the bottom layer. The required thickness ratios, along with the corresponding bending stiffness ratios for bistability, are presented in Table 2.

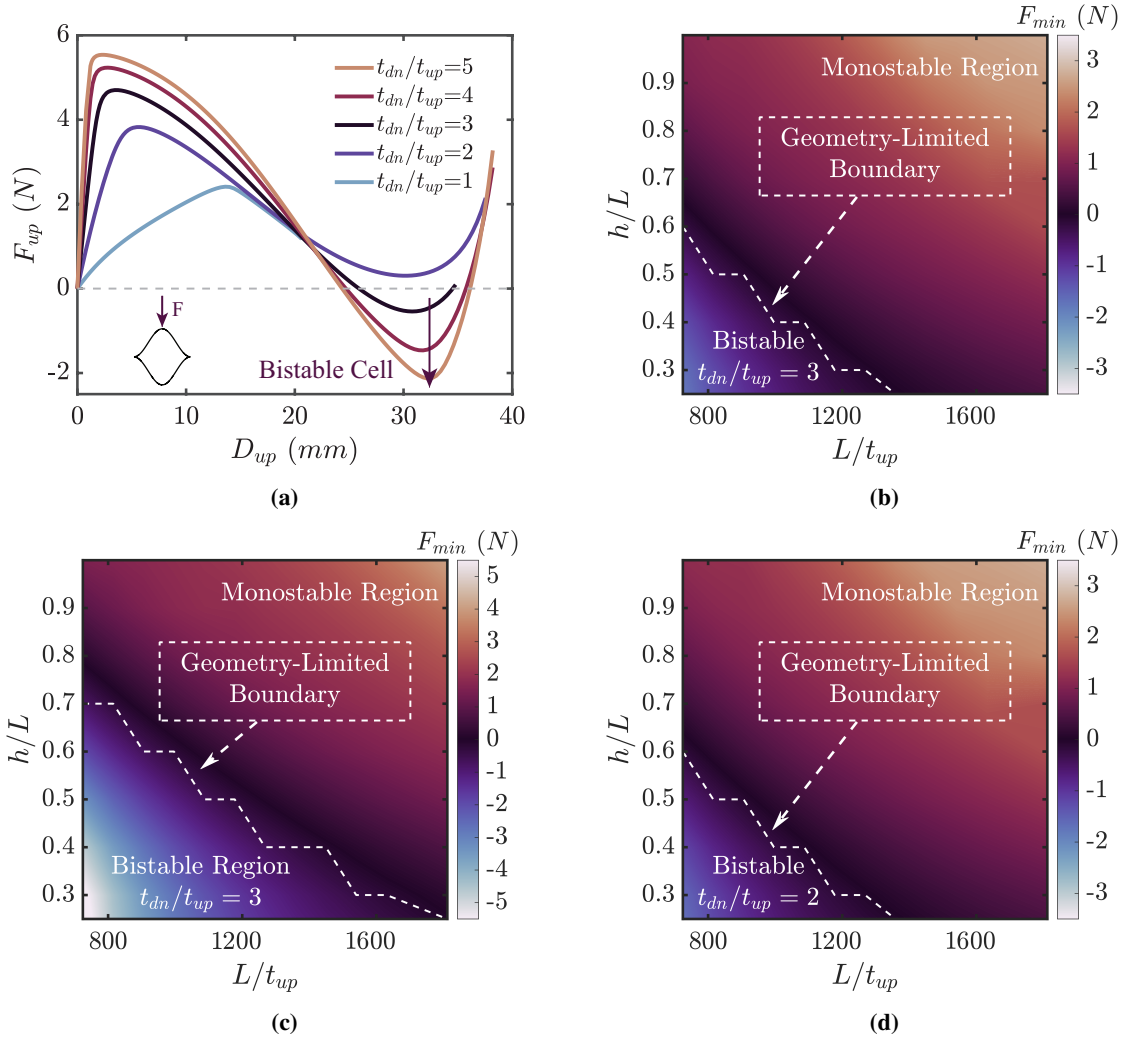


Fig. 3 (a) Bistability threshold for a GFRP unit cell. Bistability contours for (b) GFRP, (c) CFRP, and (d) hybrid unit cell with GFRP upper and CFRP lower arch.

One of the main questions to address after achieving bistability is how to measure the stability of the second equilibrium configuration. The energy barrier to transition back to the cell's initial configuration is an important indicator of stability. Here, we use the minimum reaction force (F_{min}) as a proxy for the energy barrier. In the Figures 3b, 3c, and 3d the values of F_{min} are presented for different cell aspect ratios (h/L) and slenderness (L/t_{up}) for the

critical thickness ratio leading to bistability. Python scripting was used to generate the contour plots. A For loop iterated on the cell length L from 40 mm to 100 mm in increments of 5 mm, while the cell aspect ratio was varied in a nested For loop from 0.25 to 1.0 in increments of 0.05.

Compared to GFRP, CFRP demonstrates superior resilience in the second stable configuration due to its lower F_{min} values (Figure 3c vs 3b), resulting in enhanced stability against perturbations. This property ensures that perturbations are less likely to revert the structure to its initial stable state, making CFRP more advantageous in applications requiring high stability in the second equilibrium configuration. In hybrid cells, the combination of CFRP as bottom arch and GFRP as upper arch, alters the bistability threshold from a thickness ratio of 3 to 2 while maintaining the same minimum load range (F_{min}). This behavior indicates that the material of the top layer primarily dictates the energy barrier, proportional to F_{min}, whereas the material of the bottom layer predominantly drives the critical thickness ratio required for bistability.

Table 2 The required ratios of thickness and bending stiffness for initiating bistability in a unit cell.

	t_{dn}/t_{up}	$(E_1I)_{dn}/(E_1I)_{up}$
GFRP	3	27.0
CFRP	3	27.0
Hybrid	2	25.4

The results in Table 2 demonstrate that, while the thickness ratio for the hybrid configuration decreases from 3 to 2, the bending stiffness ratio between the lower and upper arches remains nearly the same. This suggests that the critical bending stiffness ratio for both the hybrid and single-material cases may inherently converge if the thickness were allowed to vary continuously. However, due to the discrete nature of the experiment—limited to adding plies of specific thicknesses—the bending stiffness values studied are relatively limited. Nonetheless, these results indicate that the critical bending stiffness ratio could be consistent across all cases. This observation aligns with the intuition that bending stiffness is the key parameter influencing bistability thresholds.

In the analysis of bistable cells and based on the results showed in the Figure 3, it can be seen that two critical thresholds govern the structural behavior. The first is the bistability threshold, which defines the minimum bending stiffness ratio required for the existence of a second stable equilibrium state. The second is a geometry-limited bistability boundary, which constrains the cell's bistable behavior based on its geometry.

The geometry limitations of the bistable region in unit cells with higher aspect ratios and slenderness directly corresponds to unwanted cell deformations. As shown in Figure 4, the prescribed vertical displacement induced an horizontal deformation Δ_x. At higher aspect ratios (e.g., $h/L = 0.7$ in this figure), bistability is prevented by the excessive deformation of the bottom arch, which does not provide enough confining stiffness to prevent the horizontal deformation of the top arch. This is due to the high reaction force required to deform the top arch for tall cells. For more

slender structure, excessive bottom arch deformation also limits the region in which bistability is found.

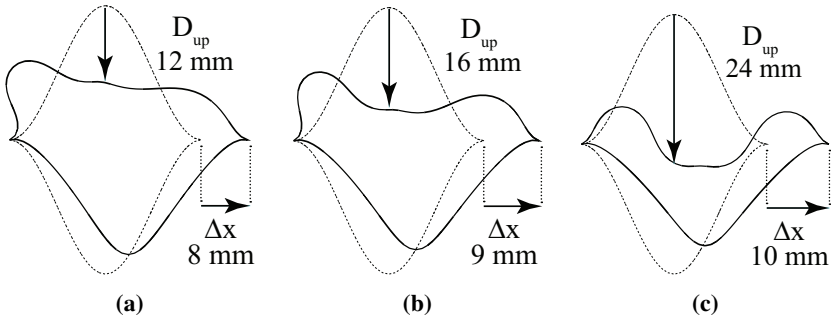
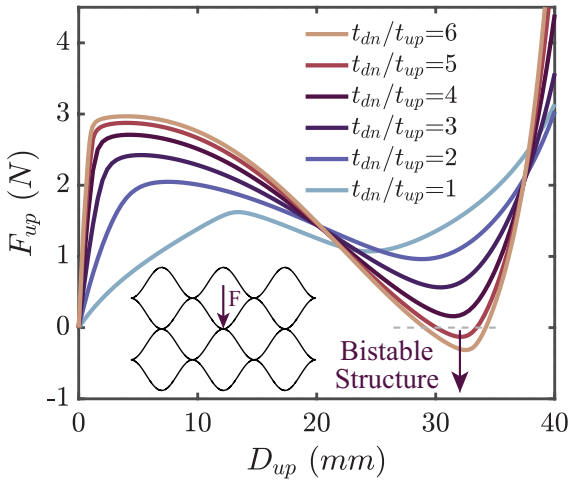


Fig. 4 Deformed shape of a high aspect ratio unit cell as the top arch displacement is increased to: (a) $D_{up} = 12\ mm$ **(b)** $\Delta D_{up} = 16\ mm$**, (c)** $\Delta D_{up} = 24\ mm$**.**

2. Multistability of Meta-structure

To investigate the bistability behavior and design considerations of meta-structures, the following analysis explores the effects of the number and architecture of cells on the bistability threshold and the resulting stable configurations.

A meta-structure consisting six cells arranged in a 3x2 array is used as a benchmark to study bistability in more complex structures. This configuration can then be tessellated to form a larger meta-structure, as described in Section II. The 3×2 cell network is chosen for this analysis because it the smallest unit that fully captures the effect of network compliance on multistability, as described in the next section. The transition between stable configurations is investigated by designating one cell as the target cell (in this case, the middle cell of the bottom row) and imposing a displacement to the top arch of that cell. This structure is made of GFRP, and the cell dimensions are the same as those mentioned for the single cell in Figure 3, namely $L = 40$ mm and $h = 20$ mm. Pinching is applied to the target cell as indicted by the arrow in the inset of Figure 5a. The bistability threshold is studied by sequentially increasing the number of plies for the lower arch of the target cell, while keeping a $[0]_1$ layup constant for the other arches, similarly to the single cell analysis. By increasing the number of plies from $[0]_1$ to $[0]_6$ for the upper arch of the target cell, it was observed that the bistability threshold for the 3x2 network occurs at a thickness ratio of $t_{dn}/t_{up} = 5$, as shown in Figure 5. In addition, the maximum strain when pinching the structure described in Section IV.A.2 is 0.63% (strain of top ply in the regions of highest curvature). Considering the maximum strain of the epoxy matrix (4.14% from the datasheet [39]) and the reported experimental range for S2 glass fibers (4.5% - 5.7%[40, 41]), the snap-through deformation of the structure is purely elastic. It is also important to note that deployable space structures can withstand high strains primarily because of their low laminate thickness. The maximum bending strain a structure can withstand when flattened is given by $\varepsilon_{max} = t/2R$, where t is the laminate thickness and R is the laminate's initial radius of curvature. For the GFRP composite used in this study, the minimum radius of curvature to avoid exceeding 4.14% strain is 0.67 mm which is significantly lower than the change in radius of curvature observed during deformation.



(a)

	Architecture	$(E_1I)_{dn}/(E_1I)_{up}$
Length effect	3x2	125
	5x2	125
	7x2	125
Row effect	5x2	125
	5x3*	216
	5x3**	216

* Applying the load in the first row (bottom row)

** Applying the load in the second row (middle row)

(more details in Figure 13)

(b)

Fig. 5 (a) Force-displacement curves in a 3×2 network. (b) Effect of total length and number of rows on bending stiffness for bistability.

The key question here is: What effect do the total length and number of rows of the meta-structure have on its bistability threshold? Based on the results reported in Figure 5b, adding cells to the network along its length does not affect the required bending stiffness ratio for achieving bistability. This indicates that the structure's length has no significant effect on the confining stiffness required for a deformed equilibrium state to arise in the target cell. There is a narrow critical region surrounding the target cell, in which additional cells affect the bistability threshold, but the size of this region of influence appears to be fully captured by a 3x2 cell network. Therefore, it can be concluded that the behavior of the 3x2 network can be generalized to larger structures with greater lengths, without changing the required bending stiffness ratio. In contrast, adding rows along the structure's height alters the behavior: The required stiffness ratio changes, and the direction and shape of the second stable configuration are also affected.

The effect of the cellular network can be qualitatively understood as follows. Cells sharing the same row as the target cells can be abstracted as springs directly acting on the target cell's supports, providing a compressive force in the longitudinal direction. Cells belonging to a different row as the target cells can be though of as transverse springs attached to the midpoint of the top arch, providing a spring force in the transverse direction. While adding compressive reaction forces in the longitudinal direction is beneficial, as it increases the confining stiffness, adding a vertical spring force at the top of the cell directly opposes the desired negative reaction force necessary for triggering bistability. Intuitively, it can be concluded that adding layers in the transverse direction would increase the equivalent transverse spring constant, thereby requiring a higher thickness ratio. This is why the required bending stiffness ratio for initiating bistability in a meta-structure with more rows ($(E_1I)_{dn}/(E_1I)_{up}$ = 216 for the 5x3 architecture) is higher than that for the previously studied networks ($(E_1I)_{dn}/(E_1I)_{up}$ = 125 for 3x2 and 5x2 architecture). When looking at the structural properties of the deformed configuration it is important to highlight that the total height of the structure

reduces which lowers its equivalent second moment of area. However, pre-stress is also introduced which partially compensate for the reduced equivalent cross-section, and we do not expect a significant change in bending stiffness between the undeformed and deformed configurations which aligns with initial experimental observations. Pure bending experiments on deformed structures are currently being conducted to quantify the deployed structural properties of these structures. However, the maximum bending moment the deformed structure can withstand is ultimately governed by the energy barrier required for cells to transform back to their initial configuration, and we anticipate a low energy barrier to be the main limitation of these structures in their deployed configuration. The simplest solution to increase the energy barrier is to increase the thickness ratio to achieve a more stable second configuration. In addition, alternative cell geometries are currently being explored to dramatically increase the energy barrier. A promising concept (beyond the scope of this paper) relies on re-entrant cell geometries that utilize contact to "jam" in their second stable configuration. In practice, increasing the energy barrier is critical to counteract inertial loads, vibrations and other perturbations on orbit.

As discussed in this section, increasing the number of rows in the structure affects its critical bending stiffness ratio, whereas increasing the number of columns does not have a significant impact. Combining this insight with the approach of pinching multiple cells (instead of just one cell) can serve as a potential design strategy to control the second stable configuration. This concept will be explored in greater detail in the next section.

B. Pinching Strategy and Scalability

In Section IV.A.2, to address the previous question regarding the impact of length and number of rows on the bistability behavior of a meta-structure, it was hypothesized that there exists a region of influence around the target cell in which neighboring cell deformations affect the target cell's bistability. Our ultimate goal is to collapse multiple cells to produce complex deformed shape, and determining whether multiple target cells can enhance or inhibit stable deformed shape is of great importance. We hypothesis that the region of influence postulated in the previous section could serve as a measure of the potential interaction between cells. To identify this critical region, we analyzed the required thickness ratio needed to produce a stable equilibrium state by collapsing target cells in two different pinching strategies.

To achieve the desired target shape, both the pinching strategy and the pinching locations play a crucial role. Two main strategies are considered here: parallel pinching (simultaneously pinching at two or more locations) and sequential pinching (pinching at each location one after the other). Our aim is to investigate the interacting between neighboring pinched cells and we hypothesize the existence of a critical region of influence for both strategies, in which the mechanical behavior of pinched cells is highly coupled.

1. Parallel Pinching

We first focus on the parallel pinching strategy to examine how the interaction between two simultaneously pinched target cells influences the system's multistability. In particular, we investigate how varying the distance between these two target cells affects the required thickness ratio and the resulting mechanical behavior.

Figure 6a illustrates how changing the distance between the two target cells influences the required thickness ratio. When the target cells are separated by more than a two-cell distance (2CD), the presence of multiple target cells does not affect the bistability behavior. However, with less than a two-cell distance, the bistability threshold occurs at a lower thickness ratio. Previous observations revealed that deformation of the bottom layer is the primary mechanism that compromises bistability. For a single target cell, when the top arch is displaced downward, the bottom arch tends to flatten (outward longitudinal deformations). This flattening is counteracted by increasing the bending stiffness of the bottom arch. When two cells are displaced simultaneously, the bottom arch of the right cell attempts to expand outward, generating a compressive force on the left target cell, and vice versa. These additional longitudinal compressive forces counteract the deformation of the bottom arches, reducing the amount of bending stiffness required to stabilize them. It was also observed that when the target cells are directly adjacent to each other (0CD), the compressive loads induced by the pinching of each cell on its neighbor significantly increases. This mutual interaction leads to highly unstable structures and loss of convergence.

Figure 6 shows the required thickness ratio to obtain bistability through parallel pinching, along with schematics of the second stable state for a one, two, and three cell distance between pinching locations. This finding aligns with the observations regarding the effect of the cell network length on bistability, and supports the idea of a critical region of influence for each target cell. If these regions overlap, the bottom arches deformation oppose each other leading to a beneficial interaction between cells. Conversely, outside this critical region, the target cells do not influence each other.

To identify the source of instabilities when pinching two adjacent cells (0CD), a buckling eigenvalue analysis was conducted. The structure is first loaded close to the point at which the solver diverges, as indicated in Figure 7 , and a linear stability is then carried out. A bifurcation is identified on the load-displacement curve, and the corresponding eigenmode features symmetry-breaking deformations which consist in a horizontal motion between top and bottom layer, as illustrated in Figure 7. It is important to mention that the deformations are infinitesimal at the bifurcation point, and the amplitude of the eigenmode plotted in the Figure does not have any physical meaning. Therefore, the self-intersections observed in Figure 7 are only an artefact of the deformation scale factor used for visualization purposes. It is also worth noting that there are no other bifurcations found in the immediate vicinity of the first bifurcation."

2. Sequential Pinching

We next investigates the sequential pinching strategy. The minimum reaction force achieved during snap-through is of particular interest since it is proportional to the energy barrier for the structure to transition back to its undeformed shape,

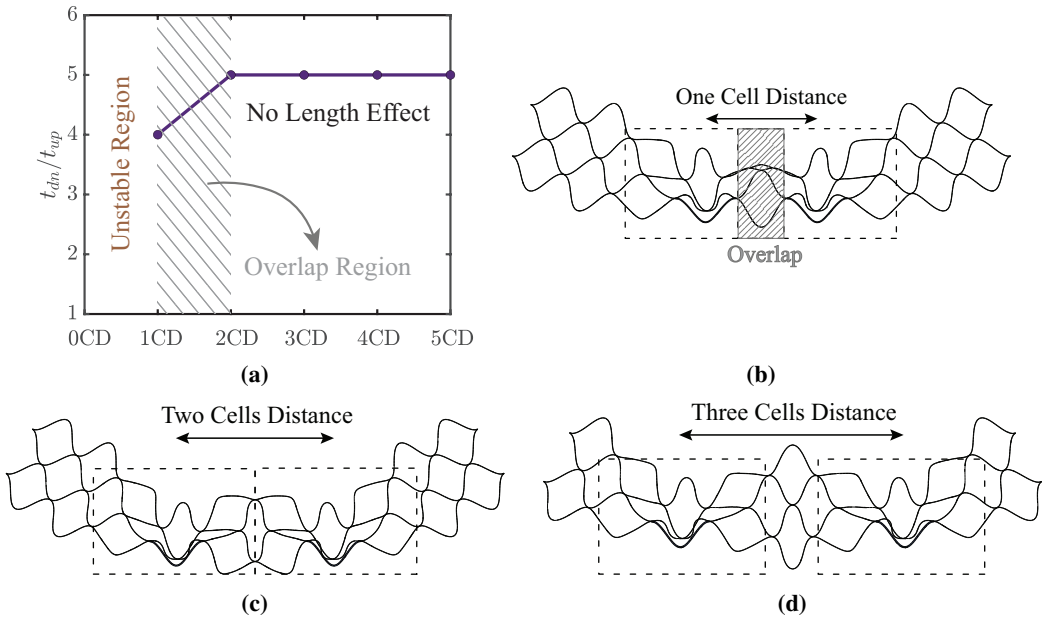


Fig. 6 (a) Required thickness ratio for bistability versus target-cell distance. (b–d) Second bistable configuration for one-, two-, and three-cell distances.

i.e. the level of stability of its second equilibrium state. The relationship between the minimum load and the distance between target cells is shown in Figure 8. Similarly to the parallel pinching strategy, reducing the spacing between pinched cells significantly alters the system's mechanical response. Similarly to the parallel pinching strategy, reducing the spacing between pinched cells significantly alters the system's mechanical response. But, in sequential pinching, an overlap between two 3x2 networks leads to a loss of bistability rather than a reduction in the required thickness ratio observed in parallel pinching. Note that for sequential pinching, this loss of stability cannot be counteracted by increasing the thickness ratio, and an updated Figure 6a for this type of pinching would give a straight line corresponding to a thickness ratio of 5 after a one-cell offset. Therefore, for sequential pinching, the minimum force at a constant thickness ratio of 5 is reported as an indicator of the bistable-to-monostable transition. Conversely, the minimum force during snap-through is not affected by the offset between pinching locations for parallel pinching. When the distance decreases to 1CD, the minimum required force becomes positive, indicating a monostable configuration, where the deformed shape is not an equilibrium state. The sequential pinching of neighboring cells (0CD) leads to the same instabilities discussed in the previous section (lateral motion and symmetry breaking) and shown in Figure 7. Consequently, the second stable configuration is difficult to achieve.

These findings, in Sections IV.B.1, and IV.B.2, confirm that multistability emerges only when the spacing between target cells exceeds a critical threshold (≥2CD), emphasizing the importance of strategic cell actuation for achieving both stable reconfiguration and desired curvature in space structure applications.

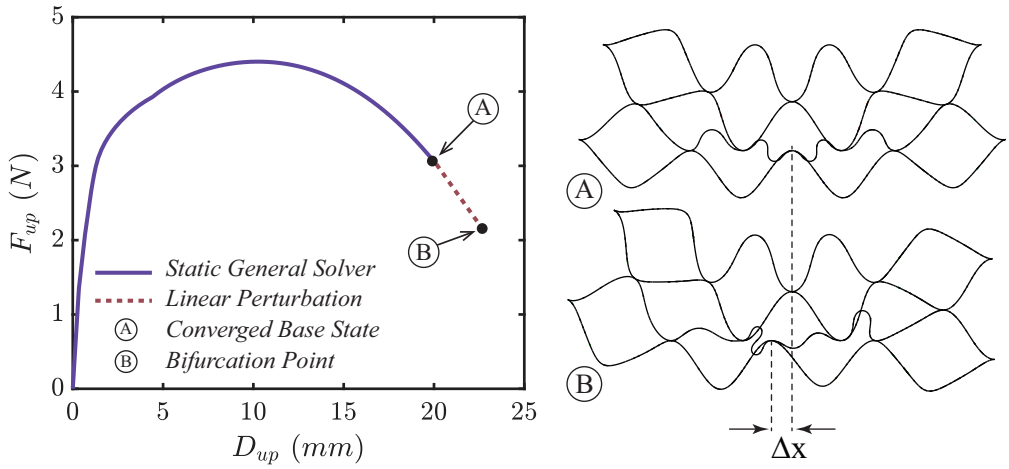


Fig. 7 Eigenvalue analysis when pinching adjacent cells (0CD), and corresponding buckling eigenvalue and eigenmode featuring lateral sliding between top and bottom cells.

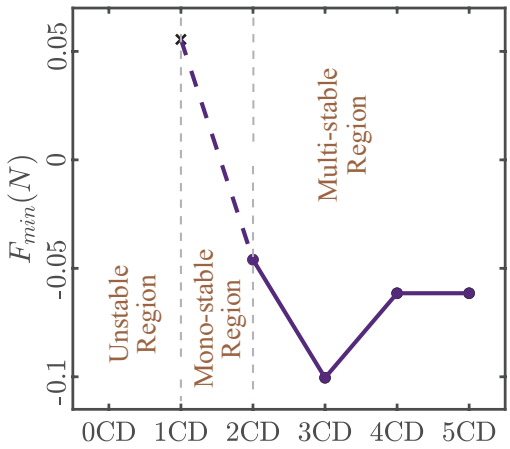


Fig. 8 Minimum reaction force of the meta-structure in sequential pinching.

3. Scalability

As described in Section II, our final goal is to create a deployable feedstock meta-structure whose shape can be programmed during deployment to design shape-changing large space structures. As an illustration, we demonstrate the formation a semi-circular structure that can for instance be tessellated to support reflectors or antennas. Considering that the second shape is a function of the number and locations of target cells, we focused on a case study of a long, 2-row boom with four target cells. As shown in Figure 9, by sequentially collapsing the target cells, a stable semi-circular shape can be achieved. For this proof of concept, the target cells are chosen such that there are no overlaps between their regions of influence, and also the critical thickness ratio is $t_{dn}/t_{up} = 5$.

After identifying the stable configurations of the meta-structure deformed via snap-through shaping, the next question is: How can we control the second stable configuration to achieve a desired shape? In other words, how can we program the shape of the structure?

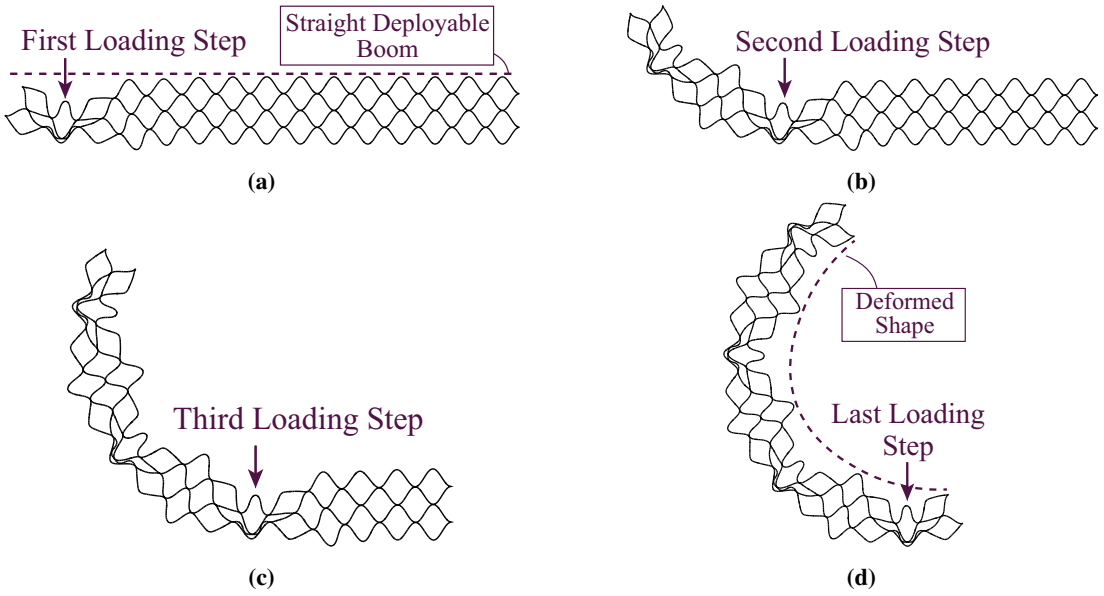


Fig. 9 Steps to change the meta-structure's global shape form straight to curved through sequential pinching.

C. Programmability

To investigate the programmability of the concept, we first analyze a longer boom to minimize the effects of boundary conditions and examine the structure's ability to generate different curvature radii. The curvature radius of a two-row boom, pinched sequentially for various cell spacings is shown in Figure 10, along with its deformed shape after pinching. The radius of curvature (R) was calculated by fitting a semi-circular arc along the inner side of the structure after deformation As discussed earlier, bistability cannot be achieved when the distance between pinched cells is less than 2CD. As the pinched cells spacing increases beyond 2CD, the average radius of curvature increases. This behavior is attributed to the larger fraction of the structure undergoing significant deformations. Such curved configurations are particularly advantageous in deployable space systems where large curved apertures lead to increase in performance, for instance in large parabolic RF antennas.

The effect of cell geometry on the end rotation generated by a 3x2 GFRP network is then calculated and presented in the contour plot in Figure 11. The end rotation corresponds to the rotation of a reference point rigidly coupled to all the nodes located on the top and bottom edges of the cell network and is expressed in degrees. The full opening angle generated by the structure corresponds to twice the end rotation presented in Figure11. This parametric study is implemented through a Python script that iterates over cell lengths from 40 mm to 100 mm and aspect ratios from 0.3 to 0.8. From this contour plot, it can be observed that, at a constant aspect ratio, the slenderness of a cell (L/t) has little effect on the amount of end rotation. Therefore, the aspect ratio is identified as the primary parameter governing both the end rotation of the network and the resulting radius of curvature. The plot further reveals three distinct regions as the aspect ratio increases from 0.3 to 0.8. The first region (approximately $0.3 - 0.45$) corresponds to lower rotations. In the

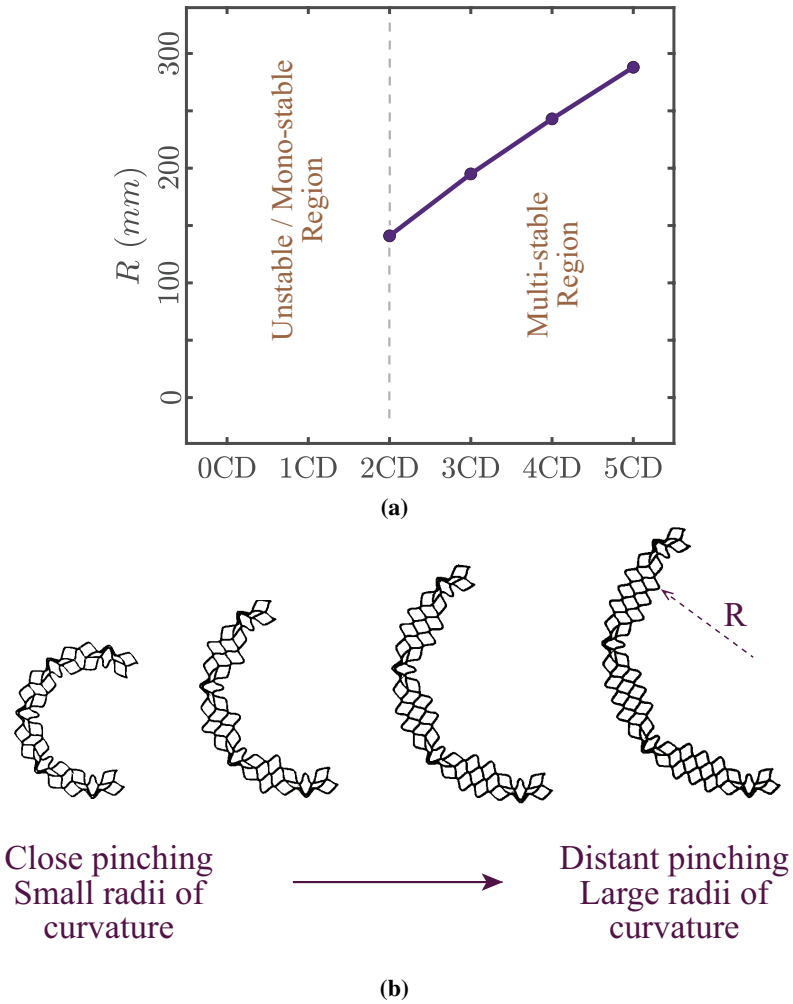


Fig. 10 (a) Radius of curvature of the deformed structure as a function of cell distance, and (b) deformed shape after pinching.

second region (0.45 − 0.6), the network exhibits maximum rotation. Beyond this, in the third region (aspect ratio > 0.6), the rotation decreases again. This indicates that there exists an optimum range of aspect ratios for achieving maximum rotation in the system, which for this network configuration is approximately 0.45 − 0.6. However, it is expected that other geometries could yield a larger modulation of end rotation that observed for the type of cells studied here.

To assess how programmable this structural concept is, in Figure 12, we considered the same two-row structure as in Section IV.B.3 with four pinching locations, but alternating pinching directions. The first and third cells are deflected downward while the second and fourth cells are deflected upward. This pinching strategy successfully produces an sinusoidal shaped boom.

Finally a three-row meta-structure is considered, as shown in Figure 13. When a cell in the first row is displaced downward, the resulting global stable shape exhibits curvature on its upper surface. By shifting the target cell to the second row, the deformed shape changes and curvature develops on the structure's bottom surface. This result suggests

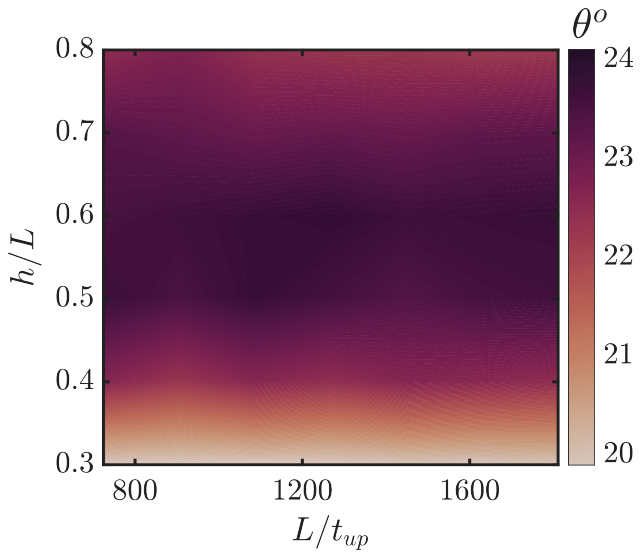


Fig. 11 Contour plot of end rotation (in degrees) for a 3×2 GFRP network

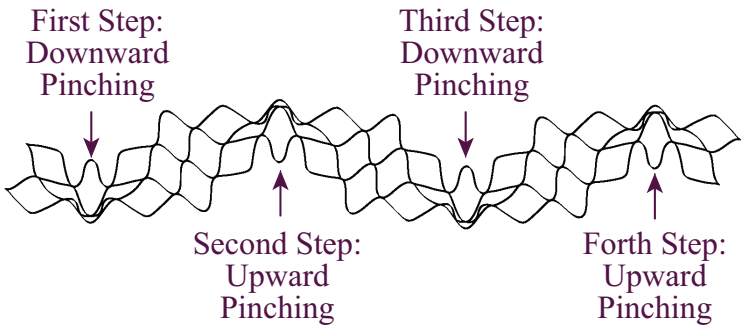


Fig. 12 S-shaped boom obtained when sequentially alternating the pinching direction.

that the deformation observed in the second stable shape is directly the result of a competition between the bending stiffness of the rows above the target cell and below the target cell. Similar to a bilayer structure, the cell network will exhibit positive curvature toward the region with lower bending stiffness.

V. Conclusion

This paper has presented a hybrid approach combining in-space deformation processing and elastic buckling to enable low-power shaping of ultra-lightweight composite cellular booms for the next generation of space structures. The concept uses bistable unit cells as building blocks for a multistable deployable meta-structure that can change shape by selectively collapsing its cells.

We first studied the bistable behavior of one single unit cell. The study revealed that although material stiffness (GFRP vs. CFRP) does not influence the required bending stiffness ratio to initiate bistability, a stiffer material (CFRP) allows bistability to be achieved at higher aspect ratios. Moreover, the study of the meta-structure showed that the second

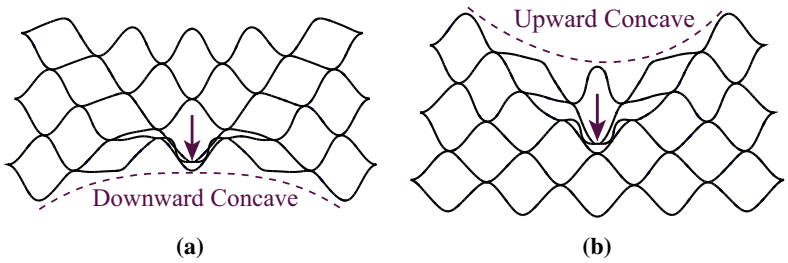


Fig. 13 Multistable meta-structure with the capability to achieve different directional shapes: (a) downward concave and (b) upward concave.

stable configuration is a function of the target cell(s) location(s), and that for each target cell, there exists a critical region in which pinching additional cells negatively affects the bistability. By investigating the effect of geometrical parameters on the bistability of these structures, we showed that while the length of the structure does not have a significant effect, the number of rows plays a crucial role in controlling the direction and deformed shape of the second stable configuration.

Furthermore, we explore the programmability of the proposed structure by analyzing the curvature radius achievable through sequential cell pinching. Our results also show that the shape of the boom can be finely tuned, enabling programmable morphologies such as S-curved booms.

The work presented in this paper can serve as a proof of concept for designing and assembling complex and large structures on-orbit. The use of elastic buckling in ultra-thin shell cellular booms enables the very low power processing of brittle ultra-lightweight composites. While this research focuses on the simulation and numerical validation of the concept for a single boom, experimental validation is currently underway and will demonstrate the shaping of a 1 m boom into a circular arch.

Acknowledgments

The authors gratefully acknowledge financial support from the New York Consortium for Space Technology Innovation and Development (NYCST).

References

[1] Gillespie, T. W., Chu, J., Frankenberg, E., and Thomas, D., "Assessment and prediction of natural hazards from satellite imagery," *Progress in Physical Geography: Earth and Environment*, Vol. 31, 2007, pp. 459–470. https://doi.org/10.1177/0309133307083296.

[2] Maiwald, V., Schubert, D., Quantius, D., and Zabel, P., "From space back to Earth: supporting sustainable development with spaceflight technologies," *Sustainable Earth*, Vol. 4, 2021, p. 3. https://doi.org/10.1186/s42055-021-00042-9.

[3] Arya, M., Lee, N., and Pellegrino, S., "Ultralight Structures for Space Solar Power Satellites," *3rd AIAA Spacecraft Structures Conference*, American Institute of Aeronautics and Astronautics, 2016, pp. 1–10. https://doi.org/10.2514/6.2016-1950.

[4] Royer, F., Zhang, J. Z., Overby, K., Zhu, E. Y., Bhundiya, H., Lang, J., and Cordero, Z. C., "Electrostatically Actuated Thin-Shell Space Structures," *AIAA SCITECH 2023 Forum*, American Institute of Aeronautics and Astronautics, 2023, pp. 1–10. https://doi.org/10.2514/6.2023-1302.

[5] Hedgepeth, J. M., "Critical requirements for the design of large space structures," *2nd Conference on Large Space Platforms: Toward Permanent Manned Occupancy in Space*, AIAA, 1981, p. 443.

[6] Dassanayake, S. P., Suh, J. E., Thomson, M. W., and Pellegrino, S., "Mass, Volume and Natural Frequency Scaling of Deployable Mesh Reflectors," *AIAA SciTech Forum and Exposition, 2024*, American Institute of Aeronautics and Astronautics Inc, AIAA, 2024, pp. 1–10. https://doi.org/10.2514/6.2024-2041.

[7] Patane, S., Joyce, E. R., Snyder, M. P., and Shestople, P., "Archinaut: In-Space Manufacturing and Assembly for Next-Generation Space Habitats," *AIAA SPACE and Astronautics Forum and Exposition*, Vol. 0, American Institute of Aeronautics and Astronautics, 2017, pp. 1–10. https://doi.org/10.2514/6.2017-5227.

[8] Patane, S., Abromitis, K., Quiros, G. A., Shestople, P., Kieler, D., and Snyder, M. P., "On-orbit Servicing, Assembly, and Manufacturing (OSAM) Enhancing Climate Research," *ASCEND 2021*, American Institute of Aeronautics and Astronautics, 2021, pp. 1–10. https://doi.org/10.2514/6.2021-4189.

[9] Bhundiya, H. G., Royer, F., and Cordero, Z., "Engineering Framework for Assessing Materials and Processes for In-Space Manufacturing," *Journal of Materials Engineering and Performance*, Vol. 31, 2022, pp. 6045–6059. https://doi.org/10.1007/s11665-022-06755-y.

[10] Nanjangud, A., Underwood, C., Rai, C. M., Eckersley, S., Sweeting, M., and Bianco, P., "Towards robotic on-orbit assembly of large space telescopes: Mission architectures, concepts, and analyses," *Acta Astronautica*, Vol. 224, 2024, pp. 379–396. https://doi.org/10.1016/j.actaastro.2024.08.022.

[11] Bhundiya, H. G., and Cordero, Z. C., "Bend-Forming: A CNC deformation process for fabricating 3D wireframe structures," *Additive Manufacturing Letters*, Vol. 6, 2023, p. 100146. https://doi.org/10.1016/J.ADDLET.2023.100146.

[12] Muench, W., "Automated beam builder," *Proceedings of the 14th Aerospace Mechanics Symposium*, NASA Langley Research Center, 1980, pp. 1–10.

[13] Kugler, J., Cherston, J., Joyce, E. R., Shestople, P., and Snyder, M. P., "Applications for the Archinaut In Space Manufacturing and Assembly Capability," *AIAA SPACE and Astronautics Forum and Exposition*, Vol. 0, American Institute of Aeronautics and Astronautics, 2017, pp. 1–10. https://doi.org/10.2514/6.2017-5365.

[14] Bhundiya, H. G., Marshall, M. A., and Cordero, Z. C., "Fabrication Time Diagrams for In-Space Manufacturing of Large Reticulated Structures," *Journal of Manufacturing Science and Engineering*, Vol. 146, 2024. https://doi.org/10.1115/1.4066721.

[15] Levedahl, B., Hoyt, R. P., Silagy, T., Gorges, J., Britton, N., and Slostad, J., "Trusselator™ Technology for In-Situ Fabrication of Solar Array Support Structures," *2018 AIAA Spacecraft Structures Conference*, American Institute of Aeronautics and Astronautics, 2018, pp. 1–10. https://doi.org/10.2514/6.2018-2203.

[16] Royer, F., Hutchinson, J. W., and Pellegrino, S., "Probing the stability of thin-shell space structures under bending," *International Journal of Solids and Structures*, Vol. 257, 2022, p. 111806. https://doi.org/10.1016/j.ijsolstr.2022.111806.

[17] Royer, F., and Pellegrino, S., "Experimentally probing the stability of thin-shell structures under pure bending," *Philosophical Transactions of the Royal Society A: Mathematical, Physical and Engineering Sciences*, Vol. 381, 2023. https://doi.org/10.1098/rsta.2022.0024.

[18] Fathi, A., Lalisani, S., and Royer, F., "Quantifying the Effect of Local Imperfections on the Buckling Energy Barrier of Thin-Shell Structures," *AIAA SCITECH 2025 Forum*, 2025. https://doi.org/10.2514/6.2025-1197.

[19] Qiu, J., Lang, J. H., and Slocum, A. H., "A curved-beam bistable mechanism," *Journal of Microelectromechanical Systems*, Vol. 13, 2004, pp. 137–146. https://doi.org/10.1109/JMEMS.2004.825308.

[20] Nadkarni, N., Arrieta, A. F., Chong, C., Kochmann, D. M., and Daraio, C., "Unidirectional Transition Waves in Bistable Lattices," *Physical Review Letters*, Vol. 116, 2016, p. 244501. https://doi.org/10.1103/PhysRevLett.116.244501.

[21] Zhang, Y., Restrepo, D., Velay-Lizancos, M., Mankame, N. D., and Zavattieri, P. D., "Energy dissipation in functionally two-dimensional phase transforming cellular materials," *Scientific Reports*, Vol. 9, 2019, p. 12581. https://doi.org/10.1038/s41598-019-48581-8.

[22] Harne, R. L., and Wang, K. W., "A review of the recent research on vibration energy harvesting via bistable systems," , 2 2013. https://doi.org/10.1088/0964-1726/22/2/023001.

[23] Zhang, Y., Tichem, M., and van Keulen, F., "Rotational snap-through behavior of multi-stable beam-type metastructures," *International Journal of Mechanical Sciences*, Vol. 193, 2021, p. 106172. https://doi.org/10.1016/J.IJMECSCI.2020.106172.

[24] Risso, G., Sakovsky, M., and Ermanni, P., "A Highly Multi-Stable Meta-Structure via Anisotropy for Large and Reversible Shape Transformation," *Advanced Science*, Vol. 9, 2022. https://doi.org/10.1002/advs.202202740.

[25] Chen, T., and Shea, K., "Computational design of multi-stable, reconfigurable surfaces," *Materials & Design*, Vol. 205, 2021, p. 109688. https://doi.org/10.1016/j.matdes.2021.109688.

[26] Shen, Z., Hu, X., Tang, Z., Xiao, Y., Wang, S., Cheng, X., and Zhang, Y., "Curvature programming of freestanding 3D mesostructures and flexible electronics based on bilayer ribbon networks," *Journal of the Mechanics and Physics of Solids*, Vol. 191, 2024, p. 105766. https://doi.org/10.1016/j.jmps.2024.105766.

[27] Udani, J. P., and Arrieta, A. F., "Taming geometric frustration by leveraging structural elasticity," *Materials & Design*, Vol. 221, 2022, p. 110809. https://doi.org/10.1016/j.matdes.2022.110809.

[28] Wu, L., and Pasini, D., "Zero modes activation to reconcile floppiness, rigidity, and multistability into an all-in-one class of reprogrammable metamaterials," *Nature Communications*, Vol. 15, No. 1, 2024. https://doi.org/10.1038/s41467-024-47180-0.

[29] Wu, L., and Pasini, D., "In Situ Activation of Snap-Through Instability in Multi-Response Metamaterials through Multistable Topological Transformation," *Advanced Materials*, Vol. 35, No. 36, 2023. https://doi.org/10.1002/adma.202301109.

[30] Mofatteh, H., Shahryari, B., Mirabolghasemi, A., Seyedkanani, A., Shirzadkhani, R., Desharnais, G., and Akbarzadeh, A., "Programming Multistable Metamaterials to Discover Latent Functionalities," *Advanced Science*, Vol. 9, No. 33, 2022. https://doi.org/10.1002/advs.202202883.

[31] Aveline, C., Thillaithevan, D., Hewson, R., and Santer, M., "Inverse Design of Snap-Through Multiscale Lattice Structures," *AIAA SCITECH 2025 Forum*, 2025. https://doi.org/10.2514/6.2025-1744.

[32] Rahman, A., Ferracin, S., Tank, S., Zhang, C., and Celli, P., "Shape-retaining beam-like morphing structures via localized snap through," *International Journal of Solids and Structures*, Vol. 300, 2024, p. 112917. https://doi.org/10.1016/j.ijsolstr.2024.112917.

[33] Santer, M., and Pellegrino, S., "Concept and Design of a Multistable Plate Structure," *Journal of Mechanical Design*, Vol. 133, 2011. https://doi.org/10.1115/1.4004459.

[34] Lalisani, S., Baxi, N. J., Abayneh, J., and Royer, F., "Snap-Through Shaping of Thin-Shell Deployable Structures," *AIAA SCITECH 2025 Forum*, American Institute of Aeronautics and Astronautics Inc, AIAA, 2025, pp. 1–10. https://doi.org/10.2514/6.2025-0690.

[35] Wilkie, W. K., "Overview of the NASA Advanced Composite Solar Sail System (ACS3) Technology Demonstration Project," *AIAA Scitech Forum*, 2021, pp. 1–10. https://doi.org/10.2514/6.2021-1260.

[36] Gdoutos, E., Truong, A., Pedivellano, A., Royer, F., and Pellegrino, S., "Ultralight Deployable Space Structure Prototype," *AIAA Scitech Forum*, 2020, pp. 1–10. https://doi.org/10.2514/6.2020-0692.

[37] Das, K., and Batra, R. C., "Symmetry breaking, snap-through and pull-in instabilities under dynamic loading of microelectromechanical shallow arches," *Smart Materials and Structures*, Vol. 18, 2009, p. 115008. https://doi.org/10.1088/0964-1726/18/11/115008.

[38] Baxi, N. J., "Snap-through Shaping of Thin-shell Deployable Structures," Ms thesis, Cornell University, 2024.

[39] PMT, "PMT-7 Technical Data Sheet," , 2017. URL https://www.patzmandt.com/_files/ugd/d12e04_26ef72a18c86473f8848da19519ac2af.pdf, accessed: 2025-09-22.

[40] Sathishkumar, T. P., Satheeshkumar, S., and Naveen, J., "Glass fiber-reinforced polymer composites - A review," , 2014. https://doi.org/10.1177/0731684414530790.

[41] Baker, A. A., and Scott, M. L., *Fibers for Polymer Matrix Composites*, American Institute of Aeronautics and Astronautics, Inc., 2016, Chap. 3, pp. 77–110. https://doi.org/10.2514/5.9781624103261.0077.0110.